Chapter 2
Shock Waves and Blast Waves

2.1 Introduction

Before introducing methods to study shock focusing, the properties behind the actual shock front should be addressed. Typically, there are two scenarios that occur depending on the method used to generate the shocks: (1) a shock front followed by constant properties lasting for some time (often referred to as a "shock wave") and (2) a shock front followed by an exponential decay in properties (often referred to as a "blast wave"); see examples in Fig. 2.1. This notation is common but erroneous since the definition of a blast wave is that of a shock wave followed by exponentially decaying properties. Thus, one has to be careful how to address what kind of shock wave scenario one is referring to. For example, the flow properties behind a shock wave produced in a constant cross-section area shock tube remain constant for an extended time period. This is not true for the flow properties behind a shock wave produced by a blast wave. The former one is a step function shown as a dashed line in Fig. 2.1. At time t_0, the pressure jumps from ambient pressure p_0 to the maximum pressure $p_{\max}$ and then remains constant. However, the pressure profile behind a shock wave created by an explosive blast wave first jumps to a peak value $p_{\max}$ and then decreases to $p_{\min}$, which is smaller than the ambient pressure. Depending on the initial charge and the distance to the explosion center, $p_{\min}$ will return to ambient pressure either gradually which is shown in Fig. 2.1 or by a secondary shock. The time duration when the pressure behind the blast remains above ambient pressure is called the positive phase (from t_0 to t^+), while the negative phase lasts from t^+ and until ambient pressure is reached. A shock wave with constant properties behind it can easily be generated using a shock tube with constant cross-section area (see more about shock tubes in Sect. 2.6.1). A shock wave with exponentially decaying properties behind it can be, for example, generated by a point source explosion in an open environment or by an open-ended shock tube where the shock wave is free to exit into an expanding volume.

N. Apazidis, V. Eliasson, *Shock Focusing Phenomena*, Shock Wave and High Pressure Phenomena, https://doi.org/10.1007/978-3-319-75866-4_2

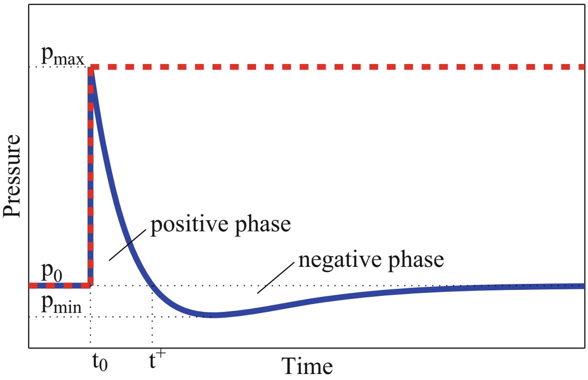

Fig. 2.1 Examples of pressure profiles behind shock waves. For constant-area shock tubes, the pressure behind the shock remains constant for some time (dashed line). For point-source explosions, the pressure profile behind the shock front decays exponentially before returning to ambient conditions (solid line)

2.2 Mathematical Description of Shock Waves

The analysis of compressible flow is based on three fundamental equations, as discussed in detail in many different textbooks in the field of fluid mechanics in general and compressible flows in particular (e.g., see Anderson (1990) [4]). The most common approach is to neglect viscosity, and then the three fundamental equations are referred to as the Euler equations of gas dynamics. They consist of conservation equations of mass, momentum, and energy presented below in differential form,

$$\frac{\partial \rho}{\partial t} + \nabla \cdot (\rho \mathbf{V}) = 0, \tag{2.1}$$

$$\frac{\partial (\rho \mathbf{V})}{\partial t} + \nabla \cdot (\rho \mathbf{V}\mathbf{V}) = -\nabla p + \rho \mathbf{F}, \tag{2.2}$$

$$\frac{\partial}{\partial t}\left[\rho\left(e + \frac{V^2}{2}\right)\right] + \nabla \cdot \left[\rho\left(e + \frac{V^2}{2}\right)\mathbf{V}\right] = -\nabla \cdot (p\mathbf{V}) + \rho\dot{q} + \rho(\mathbf{F} \cdot \mathbf{V}), \tag{2.3}$$

Here, ρ is density, t is time, $\mathbf{V} = (u, v, w)$ is the velocity vector in three dimensions, p is pressure, $\mathbf{F}$ represents body forces, e is the internal energy, and $\dot{q}$ is the heat rate added per unit mass. This system of equations is closed with an equation of state. One of the simplest equations of state one can use is the ideal gas law, which is valid for moderate temperatures and low pressures. The ideal gas law is given by

$$p = \rho R T, \tag{2.4}$$

where R is the specific gas constant and T is the temperature. There exist a number of more intricate equations of state that model more complex situations, such as low-temperature or high-pressure flows, where the intramolecular forces become important and cannot be neglected.

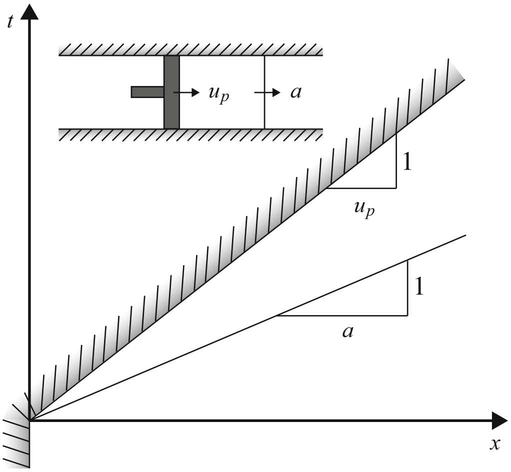

Fig. 2.2 Time-distance diagram for a one-dimensional insulated tube in which a piston is suddenly accelerated to the right with speed u_p. Two regions with uniform speed develop: one region fully affected by the piston motion and one region not at all affected by the piston motion

To illustrate the process of deriving the shock jump relations, consider an adiabatic rigid tube filled with stationary homogeneous gas with density ρ_0, pressure p_0, temperature T_0, and energy e_0. An adiabatic rigid piston is suddenly set in motion at a constant speed, u_p, that is lower than the speed of sound of the gas in the tube, a. The piston in this example is moving from the left to the right, as shown in the insert in the upper left corner in Fig. 2.2. By only considering two sets of discrete waves, one can see there will be two states with uniform speed: (1) one region of the tube is completely affected by the piston motion, and (2) one region of the tube is not at all affected by the piston motion, as illustrated in Fig. 2.2. Now, consider conservation of mass applied to a tube of length L and for a finite time interval $\Delta t = t_2 - t_1$, also illustrated in Fig. 2.3. Then one can write conservation of mass as follows:

$$\rho(L - u_p \Delta t) = \rho(L - a\Delta t) + \rho_0 a \Delta t, \tag{2.5}$$

where ρ is the density in the region bounded by the sound wave and the piston surface. Expanding Eq. (2.5) gives

$$\rho L - \rho u_p \Delta t = \rho L - \rho a \Delta t + \rho_0 a \Delta t, \tag{2.6}$$

and divide by Δt to get

$$\rho(a - u_p) = \rho_0 a, \quad \text{or} \quad a(\rho - \rho_0) = \rho u_p. \tag{2.7}$$

Finally, the result from conservation of mass can be rewritten as

$$-\frac{\Delta v}{v_0} = \frac{u_p}{a}. \tag{2.8}$$

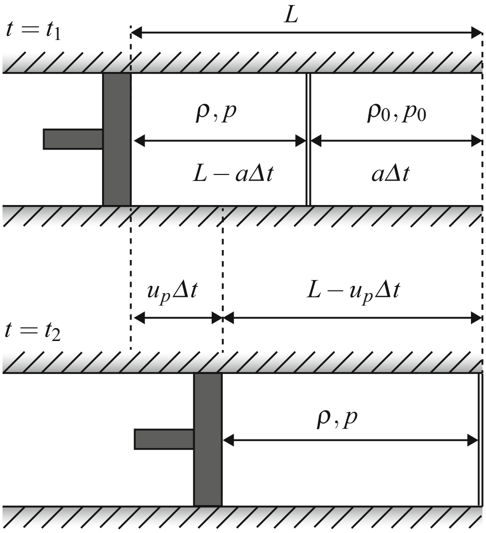

Fig. 2.3 One-dimensional insulated tubes at two separate time instants t_1 and t_2. A piston moves with constant speed u_p from left to right, and only two discrete regions are considered: one which is fully influenced by the piston motion and one region that is not at all influenced by the piston

Next, apply conservation of momentum to the same system,

$$(p - p_0)\Delta t = \rho(L - u_p\Delta t)u_p - \rho_0(L - a\Delta t)u_p, \tag{2.9}$$

and simplify this to get

$$p - p_0 = \rho(a - u_p)u_p. \tag{2.10}$$

Using the result obtained in Eq. (2.7), then Eq. (2.10) can be rewritten as

$$p - p_0 = \rho a u_p. \tag{2.11}$$

One can also show, using results obtained from conservation of mass and momentum, that the mass flux, $m = \rho_0 a$, relative to the wave is given by

$$\frac{\Delta p}{\Delta v} = -\rho_0^2 a^2 = -m^2. \tag{2.12}$$

Continuing on with conservation of energy applied to the same case as previous, we can write,

$$\rho(L - u_p\Delta t)\big(e + \frac{u_p^2}{2}\big) - \big[\rho(L - a\Delta t)\big(e + \frac{u_p^2}{2}\big) + \rho_0 e_0 a\Delta t\big] = p u_p \Delta t, \tag{2.13}$$

which, after simplification and using results obtained from conservation of mass, gives the following relationship:

$$\frac{\Delta e}{\Delta v} = -\bar{p}. \tag{2.14}$$

Here, $\bar{p}$ is the average pressure $(p + p_0)/2$ from the regions ahead and behind the propagating shock. This result is referred to as the Hugoniot equation, and it relates only thermodynamical properties across the shock wave. It is also worth noting that this relation is very general because few assumptions were made during the derivation of this mathematical expression. Therefore, it is applicable to real gases, chemically reacting gases, perfect gases, etc.

Lastly, specific enthalpy can be written as

$$\Delta h = h - h_0 = e - e_0 + pv - p_0 v_0, \tag{2.15}$$

and by introducing average specific volume as $(v + v_0)/2$, Eq. (2.15) can be rearranged as

$$\Delta h = \bar{v} \Delta p. \tag{2.16}$$

The shock jump conditions are given by Eqs. (2.8), (2.12), and (2.16). The jump conditions can be applied to a perfect gas with the ratio of specific heats denoted by γ, and the following mathematical expressions are obtained:

$$\frac{\rho}{\rho_0} = \frac{v_0}{v} = \frac{(\gamma + 1) M_s^2}{2 + (\gamma - 1) M_s^2}, \tag{2.17}$$

$$\frac{p}{p_0} = 1 + \frac{2\gamma}{\gamma + 1}(M_s^2 - 1), \tag{2.18}$$

$$\frac{T}{T_0} = \frac{h}{h_0} = \frac{p}{p_0}\frac{\rho_0}{\rho} = \left(1 + \frac{2\gamma}{\gamma + 1}(M_s^2 - 1)\right)\left(\frac{2 + (\gamma - 1) M_s^2}{(\gamma + 1) M_s^2}\right). \tag{2.19}$$

In these expressions, M_s represents the shock Mach number, and it is defined as the ratio of the speed of the shock to the speed of sound ahead of the shock ($M_s = u_s/a$). Note that Eqs. (2.17)–(2.19) are valid for a stationary normal shock in which M_s in that case is replaced by the Mach number of the incident flow upstream of the shock wave.

2.3 Mathematical Description of Blast Waves

A spherical blast wave can be generated by a point release of a large amount of energy. Because multiple expanding blast waves can be used to create shock wave focusing by letting the individual blast waves coalesce upon each other, it is useful to understand how these waves are different than those described in the previous chapter. It is also helpful to understand how the exponentially decaying properties behind the shock front can be described. One of the simplest mathematical descriptions of a blast wave is the so-called Friedlander wave form, given by

$$p(t) = p_{\max} e^{-t/t_s}(1 - t/t_s) \tag{2.20}$$

where $p_{\max}$ is the peak pressure and t_s is the time at which the pressure first becomes negative. The Friedlander wave form is also illustrated in Fig. 2.1.

Another straightforward way to mathematically describe blast waves is through the use of self-similar solutions, in which we are looking for a solution on the form $r \sim t^{\lambda}$ where λ has to be determined. This can be done in different ways, including rough estimates or dimensional analysis. Assume that a sudden release of energy $E = E_{\text{thermal}} + E_{\text{kinetic}}$ is applied to a domain with density ρ_0. The radius of the expanding shock wave as a function of time is given by $r(t)$. The mass as a function of time, $m(t)$, that is being swept up by the expanding shock wave is given by the product of density, ρ_0, and volume, V,

$$m(t) = \frac{\rho_0 4\pi r^3(t)}{3}.$$

The kinetic and thermal energy can then be estimated as follows:

$$E_{\text{thermal}} \sim \frac{3}{2} pV,$$

$$E_{\text{kinetic}} \sim \frac{1}{2} m(t) v^2.$$

Let us further assume that the shock is strong, i.e. the shock Mach number is much larger than the speed of sound, and the pressure behind the shock wave is much larger than the pressure ahead of the shock. In this case, using the shock jump pressure condition given by Eq. (2.18), along with the definition of shock Mach number $M_s = v_0/a_0$ together with $a_0 = \sqrt{\gamma p_0/\rho_0}$, the following mathematical expressions are obtained:

$$E_{\text{thermal}} \sim \frac{3}{2}\left(\frac{2\rho_0 v_0^2}{\gamma + 1}\right)\frac{4\pi r^3(t)}{3} \propto \rho_0 \frac{r^5(t)}{t^2},$$

$$E_{\text{kinetic}} \sim \frac{1}{2}\rho_0 \frac{4\pi r^3(t)}{3}\frac{r^2(t)}{t^2} \propto \rho_0 \frac{r^5(t)}{t^2}.$$

Thus, we see that both expressions are of the same type, and one can conclude that

$$r \propto t^{\frac{2}{5}}.$$

This similarity solution is often referred to as the Sedov-Taylor solution [51, 52, 56–58], and it is valid when the shock front remains strong with the assumption that the energy is released instantaneously in an infinitely small region (i.e., a point source) obeying perfect gas conditions at early times during the blast wave development. Another strong shock similarity solution was introduced by von Neumann [62] among a collection of other notable manuscripts on the topic of blast waves by Bethe and colleagues [9].

Solutions to moderate strength shocks [32] produced by point sources have been provided by theoretical means by Sakurai [48, 49] and by quasi-similarity methods by Oshima [44]. An exact solution was presented via numerical simulations by Goldstine and von Neumann [23] and analytically derived by Bach and Lee [6]. The interested reader is encouraged to further pursue these references to learn more about these other types of solutions.

2.3.1 *Initial Conditions for Blast Waves*

Assume now that we wish to prepare ourselves to study a shock focusing process for the specific case in which there are multiple blast waves that interact in such a way that a convergent shock front is created and shock focusing occurs. Furthermore, if we are interested in using numerical simulations in three dimensions to study such a scenario, then one way to initialize this simulation is to neglect the physical beginning of the blast initiation and instead start the simulation using Taylor's similarity law for point sources [57], described in brief earlier. Two advantages of computing initial conditions compared to simulating a condensed energy source directly are the following: (1) first, it eliminates the need to generate an extremely fine mesh for the blast source, and (2) in addition, sharp discontinuities at the wave front can be avoided [87]. At first, it might be easiest to start with a two-dimensional case. We can do so by using two-dimensional initial conditions that actually were modified from three dimensions by Lin [38]. In this case, Taylor's similarity law for pressure, p, density, ρ, and radial velocity, u, can be summarized as

$$\frac{p}{p_0} = {R_0}^{-3} F(\eta), \tag{2.21}$$

$$\frac{\rho}{\rho_0} = \psi(\eta), \tag{2.22}$$

$$u = R_0^{\frac{-3}{2}} \Phi(\eta). \tag{2.23}$$

Here, p_0 and ρ_0 represent the ambient pressure and density ahead of the blast wave and R_0 is the chosen radius of the blast wave front at time zero, $\eta = \frac{r}{R_0}$ with r representing the radial coordinate measured from the blast wave center. The remaining variables F, ψ, and Φ are functions of η. Applying the similarity law to the equations of motion, continuity, and equation of state for a perfect gas leads to the following three differential equations in nondimensional form,

$$\dot{\phi}(\eta - \psi) = \frac{1}{\gamma}\frac{\dot{f}}{\psi} - \frac{3}{2}\phi, \tag{2.24}$$

$$\frac{\dot{\psi}}{\psi} = \frac{\dot{\psi} + (\frac{2\phi}{\eta})}{\eta - \phi}, \tag{2.25}$$

$$3f + \eta\dot{f} + \frac{\gamma\dot{\psi}}{\psi}f(\phi - \eta) - \phi\dot{f} = 0, \tag{2.26}$$

where $f = \frac{Fa_0{}^3}{A^2}$ and $\Phi = A\phi$. The speed of sound, a_0, is the value in ambient air, and A is a coefficient that can be determined from the total energy and the shock front radius. The total energy, E, is separated into two parts, namely, kinetic energy and thermal energy, and can be written as follows:

$$\text{Kinetic energy} = 4\pi \int_0^{R_0} \frac{1}{2}\rho u^2 r^2\, dr, \tag{2.27}$$

$$\text{Heat energy} = 4\pi \int_0^{R_0} \frac{pr^2}{\gamma - 1}\, dr. \tag{2.28}$$

Expressing Eqs. (2.27) and (2.28) in terms of the variables f, ϕ, ψ, and η, the total energy E can be expressed as

$$E = 4\pi A^2\left(\frac{\rho_0}{2}\int_0^1 \psi\phi^2\eta^2\, d\eta + \frac{p_0}{a_0{}^2(\gamma - 1)}\int_0^1 f\eta^2\, d\eta\right). \tag{2.29}$$

In the early stages of the explosion, the blast wave is strong, and therefore one can assume that the pressure behind the shock front is much larger than the pressure in front of the shock, i.e., $p >> p_0$. Consequently, the boundary conditions at $\eta = 1$ can be obtained from the Rankine-Hugoniot relations

$$\frac{\rho}{\rho_0} \cong \frac{\gamma + 1}{\gamma - 1}, \tag{2.30}$$

$$\frac{U_s{}^2}{a_0{}^2} \cong \frac{(\gamma + 1)}{2\gamma}\frac{p}{p_0}, \tag{2.31}$$

$$\frac{u_s}{U_s} \cong \frac{2}{\gamma + 1}, \tag{2.32}$$

where the subscript s represents the state behind the blast and U_s is the blast wave speed. Given the total initial energy and blast radius, the three differential Eqs. (2.24)–(2.26) can then be solved numerically to obtain the needed initial conditions. These initial conditions result in a sphere of a given diameter R_0 with a moderate shock jump suitable for implementation in numerical simulations. Figure 2.4 shows line plots of nondimensional initial conditions for pressure,

Fig. 2.4 Normalized initial conditions based on Taylor's similarity law [57], reproduced from [46], with permission from Springer

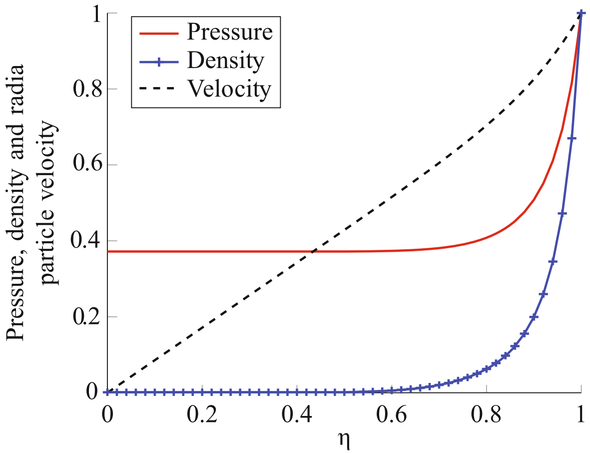

density, and radial velocity. The values are made nondimensional by scaling with the peak values at the blast wave front.

With these aforementioned equations, we can now model, in a simplified manner, the initialization of a blast wave—the first steps toward investigating shock wave focusing when utilizing blast waves. Next, we will cover the historical background and mathematical necessities to help us understand shock wave reflections.

2.4 Shock Wave Reflections

Converging shocks appear in a variety of geometrical configurations. For example, a converging shock wave may be smooth as that produced by spherical converging shocks, or it might consist of multiple planar sides and corners forming a polygonal shape. Because a converging spherical or cylindrical shock wave is unstable by nature (more on this topic in the next chapter), the converging shock wave tends to form a polygon at some instant during the shock focusing process. To better understand the shock focusing behavior, it greatly helps to be familiar with the concept of shock wave reflections, introduced next.

2.4.1 Discovery

Shock wave reflection phenomena were first reported by Ernst Mach in the 1870s [10]. Today, close to 140 years after Mach's discovery, shock wave reflection phenomena remain an active field of research that still contain many challenges left to be fully understood. During the experimental work that lead to the discovery of

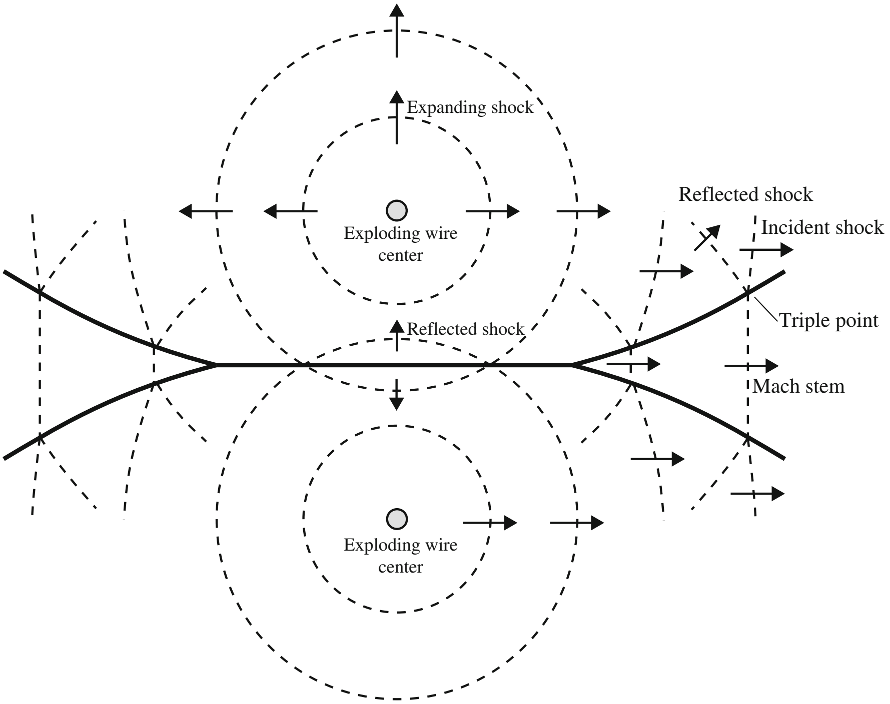

Fig. 2.5 Cartoon illustrating the resulting shock interaction that took place during Mach's experiments in the 1870s [39, 40]. Two expanding cylindrical shocks of equal strength interact and meet at the center line (thick solid line). Initially, the shocks reflect in a regular reflection pattern, but as the shocks propagate outward, the reflection pattern transition into an irregular type also referred to as a Mach reflection. Modified from [35]

what is today named the Mach wave reflection, Mach used an experimental setup consisting of two exploding wires that each produced a simultaneous expanding shock wave. As the expanding shocks collided with each other, the shock interaction began as a regular reflection but transitioned into an irregular reflection as illustrated in Fig. 2.5. Mach was able to visualize traces of the resulting shock wave interaction from the two exploding wires using a glass plate upon which a thin layer of soot had been deposited on. As commented on in the paper by Krehl and van der Geest [35], it is noteworthy to realize that Mach only saw the left behind soot trace from the path of the triple point trajectory and from there was able to piece together how the shock waves coalesced and interacted.

In an 1875 manuscript coauthored by Mach's student Wosyka [40], the irregular reflection was shown to occur in liquids. Later, Mach continued the study of two- and three-dimensional shock waves and shock wave reflection patterns [39]. Through these types of experiments, Mach visualized—for the first time—both regular and irregular reflection patterns. Fifty years later, the irregular reflection was named Mach reflection.

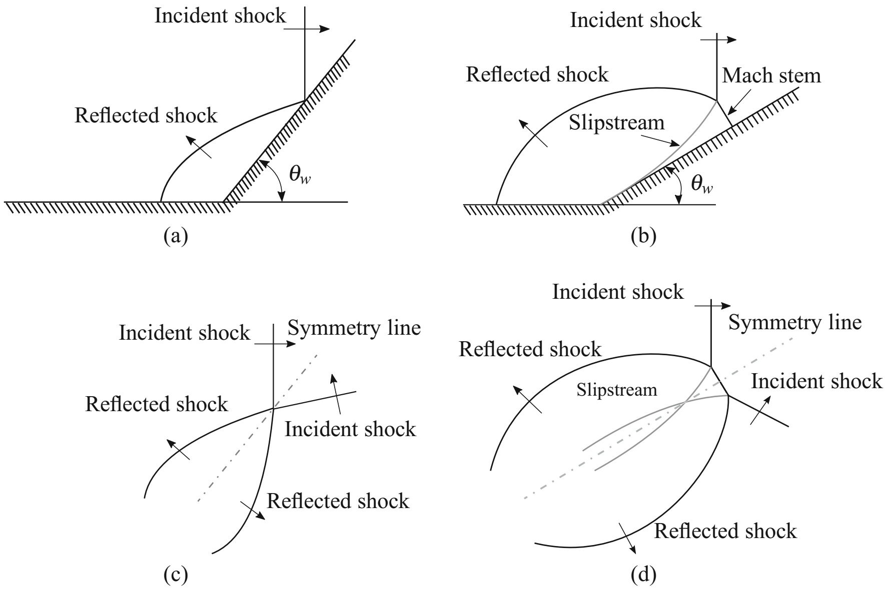

Fig. 2.6 Schematic illustration of different types of shock wave reflection configurations: (**a**) and (**c**) regular shock wave reflection configurations (RR); (**b**) and (**d**) irregular shock wave reflection configuration (IR). The top row illustrates shock reflection off an inclined wedge, and the bottom row illustrates shock reflection between two separate shock waves. Modified from [30]. (**a**) RR off a solid wedge. (**b**) IR off a solid wedge. (**c**) RR reflection between two shocks. (**d**) IR reflection between two shocks

In the early 1940s, von Neumann [61] studied shock wave reflection of a wedge. He speculated that reflected shocks could be classified into two groups based on their structure, as illustrated in Fig. 2.6a and b. The first group, regular reflection (or RR), features an incident and a reflected shock that meet at the surface of the reflecting body, shown in Fig. 2.6a. The second group, known as irregular reflection (or IR), features an incident shock and a reflected shock as well as a third shock, the Mach stem. The three shocks—and a slip line [11]—meet at a triple point located above the reflecting surface, shown in Fig. 2.6b. In the same publication, von Neumann also speculated that the Mach reflection first observed by Ernst Mach was a possible irregular reflection configuration. These two types of reflection occurrences are often referred to as two- and three-shock theory. As shown by Ernst Mach, shock reflection also occur between two separate shocks, further illustrated by the examples in Fig. 2.6c and d. To simplify, the symmetry line can be thought of as a wall assuming viscous effects of the fluid are ignored. There are many different types of irregular reflections, and the reader can refer to, for example, the very comprehensive book written by Gabi Ben-Dor [7] and subsequently updated papers by the same author [8] for a thorough description of this subject.

2.4.2 Transition from Regular to Irregular Reflection

A theoretical limit, which determines whether the reflection is regular or irregular, was derived by von Neumann [61] and is known as the detachment criterion. In pseudo-steady flow, such as the cases shown in Fig. 2.6, the shock wave configuration grows with time such that the length of the Mach stem grows gradually while following the reflecting surface. Hence, what may look like an RR configuration initially often transforms into IR configuration as the shock wave transverses the wedge. Therefore, in pseudo-steady flow, the transition angle is defined as the angle for which the reflection configuration remains RR without transforming into IR.

The transition angle, θ_{tr}, is a function of the incident shock wave Mach number, M_s, the heat capacity ratio, γ, and the deflection angle, θ_w. In short, irregular reflections are classified either as von Neumann reflection or a Mach reflection, of which many different types exist. Figure 2.7, from Ben-Dor [8], shows an example of transition boundaries and domains in air for several different types of reflections.

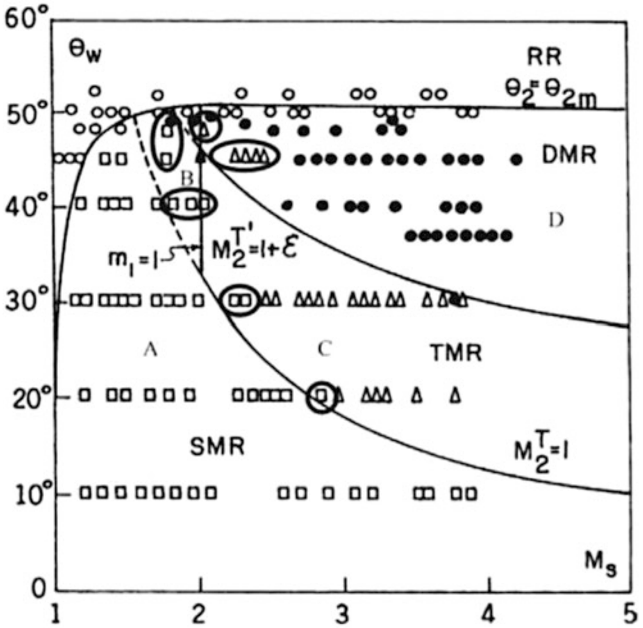

Fig. 2.7 Boundaries and domains representing the domains of single Mach reflection (SMR), pseudo-transitional Mach reflection (PTMR), transitional Mach reflection (TMR), and double Mach reflection (DMR) in the (M_s, θ_w)-plane for air. The SMR-domain is marked by A. The PTMR-domain is marked by B, the TMR-domain is marked by C, and the DMR-domain is marked by D, reproduced from [8], with permission from Springer

The theory developed in this manuscript was compared to a number of experimental results, also illustrated to some degree in Fig. 2.7. For other types of gases, see, for example, the manuscript by Semenov et al. [53] that shows transition curves for a perfect CO_2 gas with $\gamma = 1.29$.

2.5 Mathematical Description of Converging Shocks: Self-Similarity

Guderley was the first to study converging shocks, and he derived a self-similar solution for cylindrical and spherical shock waves [24]. The solution relates the radius of the converging shock as a function of time and is written as

$$\frac{r}{r_0} = \left(1 - \frac{t}{t_c}\right)^{\alpha} \tag{2.33}$$

where r is the radius of converging shock, t is the time, r_0 is the initial radius at time $t = 0$, and t_c is the time when the converging shock reaches the center of convergence. The self-similar power exponent, α, describes the strength of the convergence process. The exponent depends on the medium through and the geometry in which the shock wave is propagating. Guderley determined $\alpha \approx 0.835$ for cylindrical shock waves in air and $\alpha \approx 0.717$ for spherical shock waves in air. This self-similar constant has also been studied and recalculated by several authors using numerical simulations, analytical results, and various types of experiments, resulting in an increasing number of significant digits of the self-similar exponent. Lazarus and Richtmyer [37] provided solutions to a wide range of adiabatic exponents, which later was further expanded [36]. More recently, a comparison of the solutions of self-similar theory, geometric shock dynamics, as well that of a numerical inviscid Euler solver was presented by Hornung et al. [28, 45], showing good agreement.

We will return to this important question in the next chapter where it will be discussed in greater detail.

2.6 Experimental Methods to Study Shock Wave Focusing

Experimental techniques to study shock wave focusing include annular shock tubes, exploding wires, explosives, and lasers. In the next subsections, we will give a brief review of some of the most common techniques to study shock wave focusing.

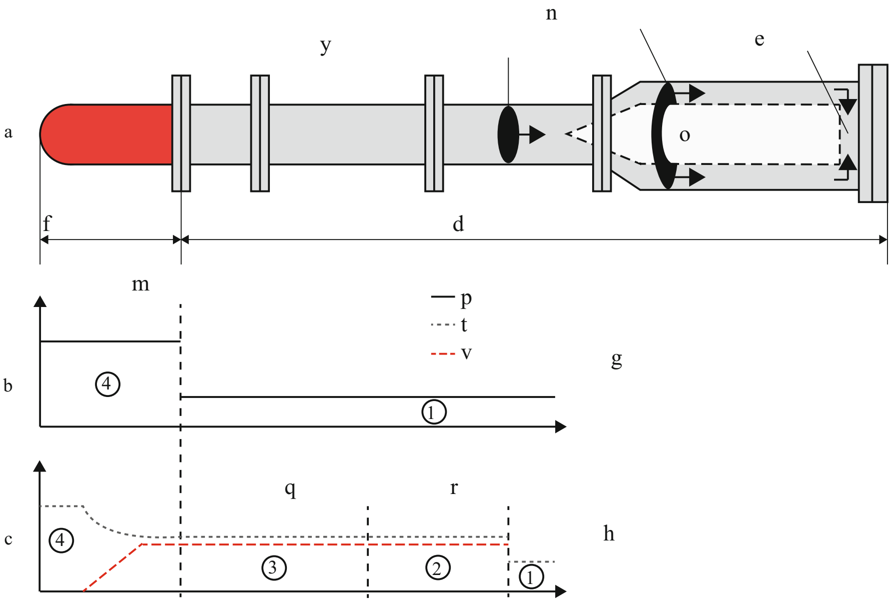

Fig. 2.8 Schematic illustration of an annular shock tube used previously in shock focusing research [13–18]. A conical insert transforms a cylindrical shock to an annular shock that is forced to converge as it enters the test section

2.6.1 *Shock Tube*

Shock tubes are perhaps one of the most common devices to study shock wave focusing. A shock tube is a tube divided into two parts, the driver and the driven sections, separated by a membrane or a fast-opening mechanical valve. Figure 2.8 shows an illustration of a typical shock tube along with the flow conditions before and after the membrane has broken. The driver and the driven sections may contain different types of gases at different temperatures. By rupturing the membrane at a desired pressure ratio, a shock wave is formed a few tube diameters downstream of the original membrane location. As the shock wave starts to propagate downstream in the shock tube, an expansion wave is propagating upstream toward the end of the driver section. The physical properties in the different regions in a shock tube are often referred to by subscript numbers; see Fig. 2.8. Very commonly, subscript 1 refers to the undisturbed region ahead of the shock wave, region 2 is the region between the shock wave and the contact surface, region 3 is the region between the contact surface (this is the boundary between the gas that was in the driver and the gas that was in the driven section of the shock tube) and the expansion fan, and region 4 represents the high-pressure region initially in the driver section. Of particular interest to any shock tube experiment is the pressure ratio across the membrane p_4/p_1, given by

$$\frac{p_4}{p_1} = \frac{p_2}{p_1}\left(1 - \frac{(\gamma_4 - 1)(a_1/a_4)(p_2/p_1 - 1)}{\sqrt{2\gamma_1}\sqrt{2\gamma_1 + (\gamma_1 + 1)(p_2/p_1 - 1)}}\right)^{\frac{-2\gamma_4}{\gamma_4 - 1}} \tag{2.34}$$

in which the ratio p_2/p_1 is the shock strength. Once the shock strength is known, it is a straightforward procedure to calculate the other thermodynamic properties across the shock using shock jump conditions introduced earlier in this chapter. It should also be noted that the pressure and velocity have to be the same on both sides of the contact surface, i.e.,

$$u_2 = u_3 \quad \text{and} \quad p_2 = p_3.$$

Directly behind the expansion wave, properties in region 3 can be found through the isentropic relations

$$\frac{p_3}{p_4} = \left(\frac{\rho_3}{\rho_4}\right)^{\gamma} = \left(\frac{T_3}{T_4}\right)^{\frac{\gamma}{\gamma-1}}.$$

As for accessing the local properties inside the expansion fan, the method of characteristics can be used, and details of such steps are outlined in many textbooks; see, for example, the book by Anderson [4].

In general, shock tubes can be horizontal, vertical, or tilted at different angles. They can be large or very small. For example, the T5 shock tunnel at Graduate Aerospace Laboratories at California Institute of Technology used to study high enthalpy flows is over 50 m long, and part of the shock tunnel consists of a 12 m long shock tube with an inner diameter 90 mm [27]. On the other hand, shock tubes used to study turbulent mixing can be as small as just a few millimeters long [67].

To create shock focusing using a conventional shock tube, an annular insert (often designed to maintain a constant cross-section area for the fluid flow) can be inserted at the end of the driven section. This method was first employed in the groundbreaking work of Perry and Kantrowitz and has later been used in many other setups; an example is illustrated in Fig. 2.8. This annulus helps to break up an initially circular shock front into an annular shape that can be forced to focus onto itself by geometrical means.

2.6.2 *Exploding Wire*

Another experimental approach to study shock wave focusing is to use an exploding wire. Exploding wires have been used for a variety of research studies dating back all the way to 1773 [41, 43]. As described earlier in this chapter, during the experimental work that lead to the discovery of the Mach wave reflection, Ernst Mach used an experimental setup consisting of two exploding wires. During the early twentieth century, exploding wires were also used for research pertaining to thin metal films [59] and spectral studies [1–3]. In 1959, the first schlieren visualizations of shock waves generated by exploding wires were presented [50], but the use of exploding wires for the study of shock wave dynamics was largely unexplored until the early 1990s [26].

Examples where shock wave focusing has been performed using exploding wires include two-dimensional cavities in which the exploding wire is located at the center of the cavity by, for example, the research group of Apazidis [5]. As the wire explodes, an expanding shock wave is created. The shock wave propagates outward and reflects off the boundary of the cavity. As the shock is reflected, it will approach the center of the cavity due to shock focusing motion. A possible drawback of this approach is that the disturbance that is created by the discharge of the exploding wire occurs at the focal point. Thus, the visibility at the focal point is decreased and one cannot properly follow the later stages of the converging shock as it propagates towards the focal point. Therefore, it is nearly impossible to study the shock wave behavior close to the focal point.

Shock focusing created by multiple exploding wires has been performed in liquid environments mainly with the purpose of studying high-energy density physics phenomena [20]. In these studies, underwater shock focusing was successfully generated by an array of exploding wires and resulted in pressures on the order of hundreds of gigapascal at the implosion center [12, 21, 33, 34, 60]. The drawback from this setup is its very limited physical size, with an initial converging shock radius of about 10 mm—leading to extreme demands on both spatial and temporal resolution on any imaging devices needed to study the focusing phase and the intricate dynamics of the shock wave.

Exploding wires have also been used to create multiple synchronized shock waves in air [19]. This particular setup, illustrated in Fig. 2.9, was used to study shock focusing from multiple synchronized shocks both in two dimensions by using longer straight copper wires to create cylindrical expanding shocks and in three dimensions by using shorter, looped, copper wires to create spherical shocks. The setup featured five high-voltage capacitors connected in parallel with a total capacitance of 1.3 μF and a maximum charge of 30,000 V. Experiments were performed with stored energies of over 400 J that were released within 2 μs. This type of research then utilizes shock focusing created by the interaction of multiple shock waves and provides an easy method to probe different types of shock focusing events in two or three dimensions.

Another method, used in the same manner as the single exploding wire technique, to generate shock focusing is by the use of electric spark discharge. However, this technique often results in similar limitations as the single exploding wire technique [5, 70] in which the light emission from the electric spark discharge prohibits visualization of the converging shock wave as it approaches the focal region.

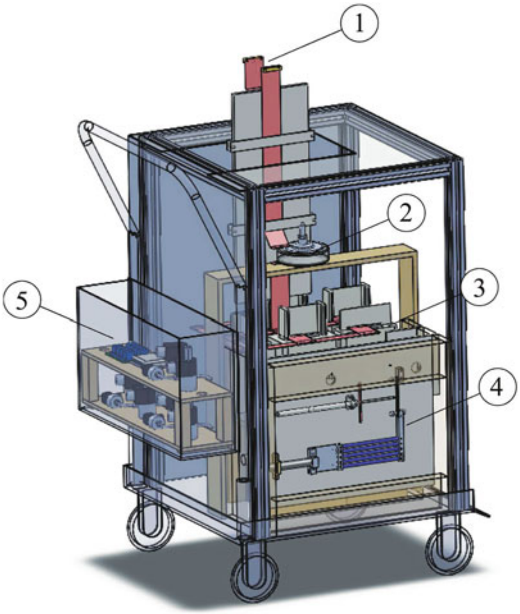

Fig. 2.9 Example of an exploding wire setup used by Eliasson and Gross [19]: (1) location of Cu-wire(s), (2) spark gap, (3) five Maxwell-type capacitors in parallel with a capacitance of 1.3 µF, (4) safety controls, (5) low-voltage controls and valves, and (6) pneumatic safety controls

2.6.3 Micro Explosives

Hosseini and Takayama [29] used a three-dimensional chamber to study shock focusing. Positioned in the middle of the chamber was a silver azide pellet (AgN3, 99.9% purity; 3.77 g/cm^3, Chugoku Kayaku Co. Japan), and depending on the type of experiment, the silver pellet mass was varied from 1.0 to 10.0 mg to create shocks of varying strengths. The 10 mg charges had a cylindrical shape of 1.5 mm diameter and were 1.5 mm long. The silver pellet was glued to the polished end of a 0.6 mm core diameter optical fiber. To initiate the explosion, the silver charges were ignited by irradiation of a pulsed Nd:YAG laser beam (1064 nm wavelength, 7 ns pulse duration, 3.2 mm diameter beam, and total energy 25 mJ per pulse). The initial shape of the expanding shock wave was not spherical, but due to the stability of expanding spherical shocks (to be discussed in more detail in the next chapter), the irregular geometry soon took on a spherical shape. It should also be noted that small fragments from the pellet explosion overtook the expanding shock wave, Fig. 2.10.

2.7 Visualization Techniques

The most common visualization techniques to study shock wave dynamics in general, and shock focusing in particular, are various types of schlieren techniques and interferometry techniques. Some of these are described next.

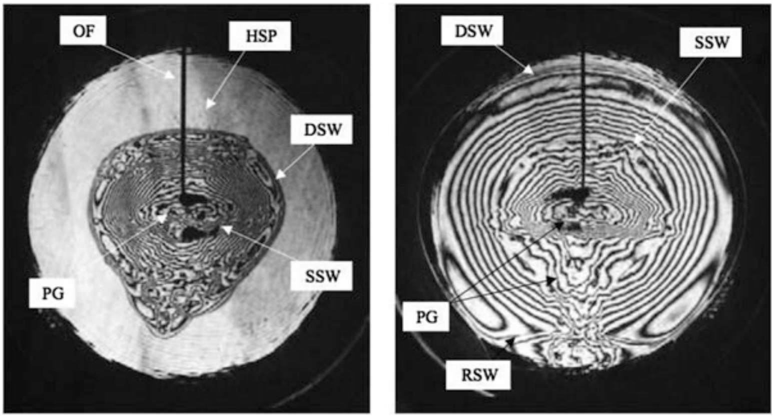

Fig. 2.10 Example of the initial (50 µs) and later stages (100 µs) of a diverging shock wave (DSW) created by a micro-explosive setup. The photos show infinite fringe interferograms produced by the explosion of a 10.0 mg cylindrical silver azide charge at an ambient pressure of 100.2 kPa. Abbreviations: *HSP* high-speed particles, *OF* optical fiber, *PG* product gases, *SSW* secondary shock wave, *RSW* reflected shock wave, reproduced from [29], with permission from Cambridge University Press

2.7.1 Schlieren Technique

Schlieren techniques are often used when visualizing shock waves in different media and for a wide range of scenarios. Although, most schlieren methods are rarely used for quantitative measurements of density gradients but are very useful for the qualitative understanding of the overall flow dynamics [13].

Optical methods for inhomogeneous media have been used since the 1600s. In the early 1670s, Robert Hooke (1635–1703) demonstrated a simple version of what is known today as the shadowgraph method to observe the convective plume of a candle for several members of the Royal Society. Christiaan Huygens (1629–1695) invented a version of the schlieren technique to look for striae in glass blanks prior to making lenses from them. Jean Paul Marat (1743–1793) published the first shadowgram of thermal plumes from hot objects. Marat did not connect the thermal plumes with density gradients of a fluid; instead he interpreted it as a proof of an “igneous fluid.” The invention of the schlieren imaging technique is usually attributed to August Toepler (1836–1912), who named the technique after the German word for optical inhomogeneities in glass: “Schlieren”. He used a light source, a knife edge, and a telescope, not too different from today’s most common schlieren setups. Ernst Mach (1838–1916) confirmed in 1877, by using schlieren optics, that nonlinear waves of finite strength could travel faster than the speed of sound, as earlier predicted by Riemann (1860). Since then, many gas dynamics phenomena have been visualized by the schlieren image technique. For a historical outlook and a detailed description of the schlieren optics method and its variations, see the excellent compilation by Gary Settles [54].

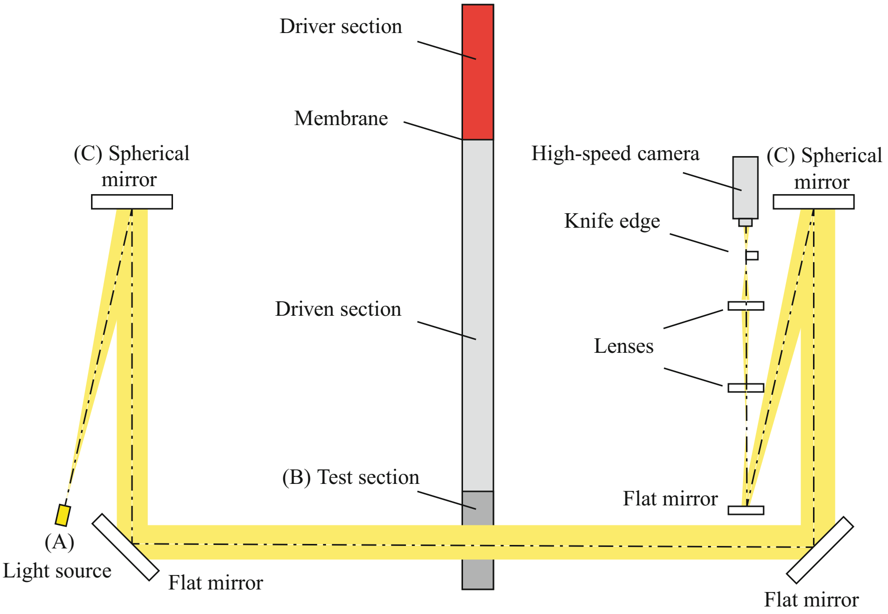

Fig. 2.11 Example of a Z-folded schlieren setup used to record high-speed photographs of shock wave dynamics in air and water in [31, 64, 65]

So, how does the schlieren system work? In short, one can describe the general idea of the schlieren system as follows: first, produce a parallel light that goes through an area of interest in which, e.g., a shock wave will occur. Then, by physics laws, we know that both the speed of light, c, and the refractive index, n, will vary with the density, ρ, of the medium in which the light is passing through. Thus, light that is passing through a region of compressible flow will be diffracted due to the density changes in the medium. The final schlieren image is obtained by cutting off part of the diffracted light before the light reaches the registry device (e.g., the camera) and thus produce darker (or brighter) regions on the photograph. If the density change takes place over a distance which is less than the wavelength of the light, then the optical method is sufficiently accurate.

One example of a schematic diagram of the so-called Z-folded schlieren method is shown in Fig. 2.11. A light source is placed at (A), which is located at a distance away corresponding to the focal length from the first concave mirror. Then, the parallel light exiting the concave mirror is reflected off two planar mirrors to enter through the test section, labeled (B), in which the event of interest will take place. After the second concave mirror, labeled (C), the light will focus, and that is the location on which a schlieren edge will be placed to cut off parts of the light. Depending on how the light is intercepted, and by how much, it will appear darker or brighter at the image plane of the test section. The most commonly used schlieren edge is a straight edge, which shows the density gradient in the flow normal to the edge. Usually, a knife edge is placed normal or parallel to the flow direction.

It is possible to change the schlieren edge into other shapes to enhance various properties. For example, a dark-field edge produces bright higher-order features against a dark background. The dark-field filter can be set up by a spherical schlieren edge, e.g., a pinhead. After the schlieren edge, different types of optics may be used to obtain an optimal image for the recording device.

The quality and the properties of the light source are of high importance for the quality of the final schlieren photograph. Usually, incandescent lamps, flash lamps, or lasers are used as light sources; see e.g., [54]. Lasers, even though usually quite expensive, are and not necessarily better for schlieren imaging. The typical schlieren concept deals with a light source composed of individual rays that do not interact with any other rays. This is not true for a laser because it produces a parallel, monochromatic, and coherent light. A common problem is that schlieren systems with coherent laser light sources become schlieren interferometers. There are workarounds to make schlieren systems work well with laser light, and some of the solutions incorporate the use of a spatial filter (i.e., pinhole) to remove interference patterns in the laser beam.

There exists several different types of "flavors" of schlieren techniques, which are often used to obtain higher levels of quantitative data. One example is the background oriented schlieren (BOS) technique, which will be introduced next.

2.7.2 Background Oriented Schlieren

Readers familiar with particle image velocimetry (PIV) will recognize parts of this chapter. The main difference is that the particles that are monitored to find displacements are stationary in the case of BOS, while in PIV applications most often the fluid flow is seeded with moving particles.

The principle of BOS is illustrated in Fig. 2.12. The camera is focused onto the background plane which has certain prescribed patterns [25]. The sample placed in between the background plane and the imaging device serves as a transfer channel function [42]. The variation of the sample's index of refraction causes a deflection angle of the originally parallel light, which leads to the displacement of the original background on the image plane of the camera; see the enlarged view in Fig. 2.12. By comparing the images obtained with and without the sample, the information about the transfer channel function or the change of index of refraction in the sample can be extracted. The deflection angle α is a key quantity, which connects the measurable displacement y' and the unknown index of refraction, n. Here, for simplicity, only the displacement in the y-direction is considered. Two relationships can be obtained for the deflection angle α. First, by assuming that the angle α is small, α can be expressed by y' and additional experimental parameters as

$$\alpha = \frac{y'}{Z_a + Z_b/2}. \tag{2.35}$$

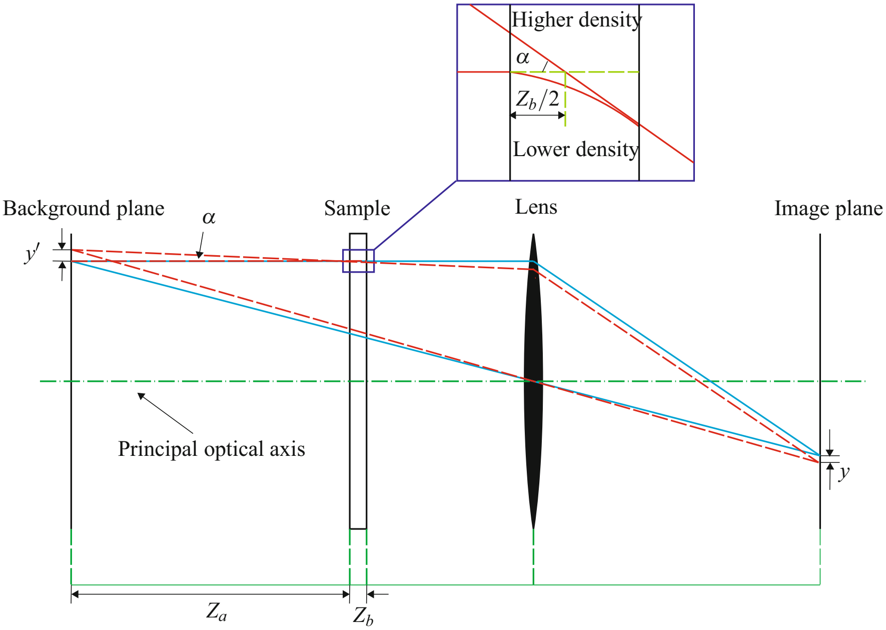

Fig. 2.12 Demonstration of the BOS principle and the key quantities. The distance between the background and sample is denoted Z_a. The thickness of the sample is Z_b. The displacement of the background observed at the image plane is given by y, and y' is the projected displacement at the background plane, reproduced from [63], with permission from Springer

In Eq. (2.35), Z_a is the distance between the background plane and the sample, and Z_b is the thickness of the sample. By increasing Z_a, the error in determining the angle α can be reduced. Second, based on Snell's law, α and the index of refraction n have the following relationship:

$$\alpha = \frac{1}{n_0} \int_{Z_a}^{Z_a+Z_b} \frac{\partial n}{\partial y}\, dz. \tag{2.36}$$

By combining Eqs. (2.35) and (2.36) and assuming the width of the sample Z_b is much smaller than Z_a, $Z_b \ll Z_a$, the following can be obtained:

$$\frac{\partial n}{\partial y} = \frac{n_0 y'}{Z_b(Z_a + Z_b/2)}. \tag{2.37}$$

The assumptions made above transform the problem into two dimensions, which means that the density is only a function of the x and y coordinates but remains constant along the z direction. The medium can be anything as long as it is possible to find a relation between density and index of refraction. For example, if the medium is water, one example of a direct relationship between the density and index of refraction is given by Yadav et al. [66],

$$n = n_0 + \kappa(\rho - 0.99824), \tag{2.38}$$

in which n_0 equals to 1.332 and κ equals to 0.322. Equation (2.38) is also referred as Gladstone-Dale relation [22]. Equation (2.38) can then be substituted into Eq. (2.37) to yield a relationship between ρ and y' given by

$$\frac{\partial \rho}{\partial y} = \frac{n_0 y'}{\kappa Z_b (Z_a + Z_b/2)}. \tag{2.39}$$

Since y' is directly measurable, it is evaluated through the displacement of the background on the image plane y. The magnification factor M is defined as

$$M = y/y'. \tag{2.40}$$

Equation (2.39) can be rewritten using M and y as

$$\frac{\partial \rho}{\partial y} = \frac{n_0 y}{M \kappa Z_b (Z_a + Z_b/2)}. \tag{2.41}$$

As seen in Eq. (2.41), the unknown ρ is directly related to y, which can be readily obtained through the analysis of experimental image data. To solve the complete two-dimensional problem instead of the simplified one-dimensional version, a Poisson equation of the density distribution can be formulated as

$$\frac{\partial^2 \rho(x, y)}{\partial^2 x} + \frac{\partial^2 \rho(x, y)}{\partial^2 y} = k\left(\frac{\partial u(x, y)}{\partial x} + \frac{\partial v(x, y)}{\partial y}\right), \tag{2.42}$$

$$k = \frac{n_0}{M \kappa Z_b (Z_a + Z_b/2)}. \tag{2.43}$$

In Eq. (2.42), $u(x, y)$ and $v(x, y)$ are the displacements of the background in x and y directions at location (x, y) on the image. Finally, since the displacements are found, any other quantity of interest can be worked out.

2.7.3 Double Exposure Holographic Interferometry

Double exposure holographic interferometry is an optical technique that allows for visualization of density changes. It has been used frequently by the research groups at, among others, RWTH Achen in Germany and the Institute of High Speed Mechanics at Tohoku University in Japan. An example of the experimental setup from each place is shown in Fig. 2.13, from [55]. As explained in [55], one clear

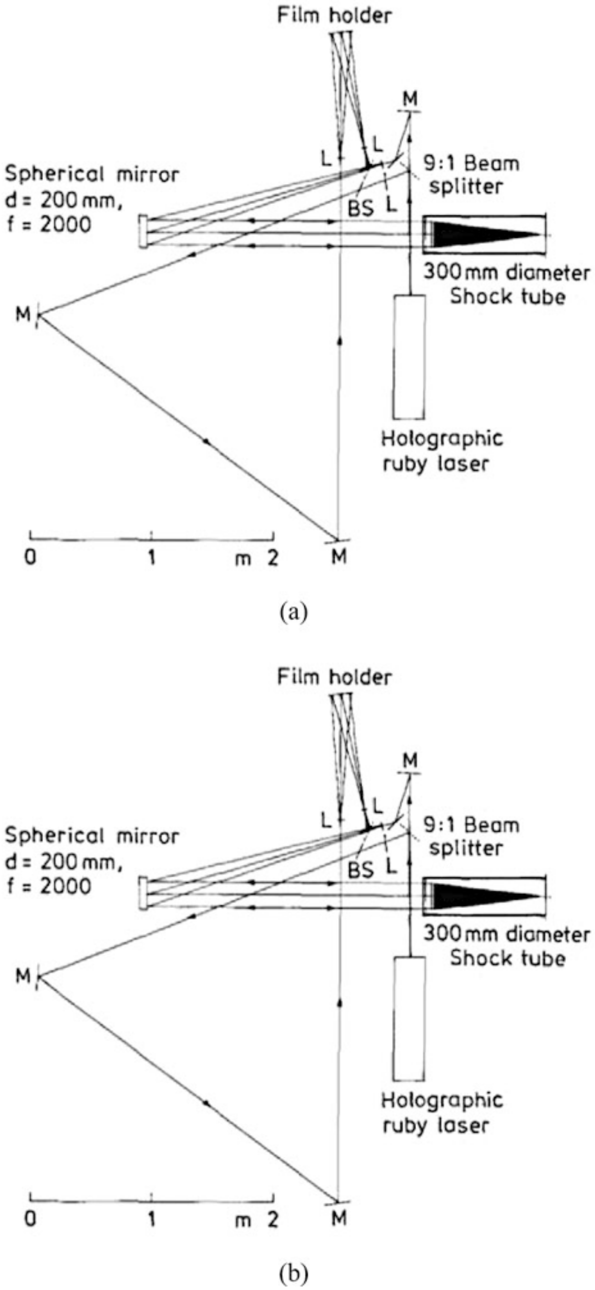

Fig. 2.13 Example of a double exposure holographic interferometry setup at (**a**) Stoßwellenlabor at RWTH Achen, Germany, and (**b**) Institute of High Speed Mechanics at Tohoku University in Japan, reproduced from [55], with permission from Springer

advantage of this method is that larger diameter visualization areas can be obtained because the restrictions on the quality of the optical elements are less stringent than for many other techniques.

References

1. Anderson, J.A.: The spectrum of electrically exploded wires. Astrophys. J. **51**, 37–48 (1920)
2. Anderson, J.A.: The spectral energy distribution and opacity of wire explosion vapors. Proc. Natl. Acad. Sci. U.S.A. **8**, 231–232 (1922)
3. Anderson, J.A.: Electrically exploded wires. In: International Critical Tables. McGraw-Hill, New York (1934)
4. Anderson, J.D. Jr.: Modern Compressible Flow: With Historical Perspective. McGraw-Hill, New York (2003)
5. Apazidis, N., Lesser, M.B., Tillmark, N.T., Johansson, B.: An experimental and theoretical study of converging polygonal shock waves. Shock Waves **12**, 39–58 (2002)
6. Bach, G.G., Lee, J.H.S.: An analytical solution for blast waves. AIAA J. **8**(2), 271–275 (1970)
7. Ben-Dor, G.: Shock Wave Reflection Phenomena. Springer, Berlin (1991)
8. Ben-Dor, G.: A state-of-the-knowledge review on pseudo-steady shock-wave reflections and their transition criteria. Shock Waves **15**, 277–294 (2006)
9. Bethe, H.A., Fuchs, K., Hirschfelder, J.O., Magee, J.L., von Neumann, J.: Blast wave. Technical report, Los Alamos Scientific Laboratory (1958)
10. Blackmore, J.T.: Ernst Mach; His Work, Life, and Influence. University of California Press, Los Angeles (1972)
11. Courant, R., Friedrichs, K.O.: Supersonic Flow and Shock Waves. Springer, New York (1948)
12. Efimov, S., Fedotov, A., Gleizer, S., Gurovich, V.T., Bazalitski, G., Krasik, Y.E.: Characterization of converging shock waves generated by underwater electrical wire array explosion. Phys. Plasmas **15**(11), 112703–112706 (2008)
13. Eliasson, V.: On focusing of shock waves. Ph.D. thesis, The Royal Institute of Technology, Stockholm, Sweden (2007)
14. Eliasson, V., Apazidis, N., Tillmark, N.T., Lesser, M.B.: Focusing of strong shocks in an annular shock tube. Shock Waves **15**, 205–217 (2006)
15. Eliasson, V., Apazidis, N., Tillmark, N.T.: Shaping converging shock waves by means of obstacles. J. Vis. **9**, 240 (2006)
16. Eliasson, V., Apazidis, N., and Tillmark, N.: Controlling the form of strong converging shocks by means of disturbances. Shock Waves **17**, 29–42 (2007)
17. Eliasson, V., Tillmark, N, Szeri, A.J., Apazidis, N.: Light emission during shock wave focusing in air and argon. Phys. Fluids **19**, 106106 (2007)
18. Eliasson, V., Kjellander, M., Apazidis, N.: Regular versus Mach reflection for converging polygonal shocks. Shock Waves **17**, 43–50 (2007)
19. Eliasson, V., Gross, J.: Experimental investigation of shock wave amplification using multiple munitions. In: Ben-Dor, G., Sadot, O., Igra, O. (eds.) 30th International Symposium on Shock Waves, vol. 2. Springer, Cham (2017)
20. Fedotov, A., Grinenko, A., Efimov, S., Krasik, Y.E.: Generation of cylindrically symmetric converging shock waves by underwater electrical explosion of wire array. Appl. Phys. Lett. **90**(20), 201502–3 (2007)
21. Gilburd, L., Efimov, S., Fedotov Gefen, A., Gurovich, V.T., Bazalitski, G., Antonov, O., Krasik, Y.E.: Modified wire array underwater electrical explosion. Laser Part. Beams **30**(02), 215–224 (2012)
22. Gladstone, J.H., Dale, T.P.: Researches on the refraction, dispersion, and sensitiveness of liquids. Philos. Trans. R. Soc. Lond. **12**, 448–453 (1863)

23. Goldstine, H.H., von Neumann, J.: Blast wave calculation. Commun. Pure Appl. Math. **8**(2), 327–353 (1955)
24. Guderley, G.: Starke kugelige und zylindrische Verdichtungsstöße in der Nähe des Kugelmittelpunktes bzw. der Zylinderachse. Luftfahrt Forsch. **19**, 302–312 (1942)
25. Hartberger, J.E.: Background-oriented schlieren pattern optimization. Master's thesis, Air Force Institute of Technology, Wright-Patterson Air Force Base, Ohio, Dec. (2011)
26. Higashino, F., Henderson, L.F., Shimizu, F.: Experiments on the interaction of a pair of cylindrical weak blast waves in air. Shock Waves **1**(4), 275–284 (1991)
27. Hornung, H., Sturtevant, B., Bélanger, J., Sanderson, S., Brouillette, M., Jenkins, M.: Performance data of the new free-piston shock tunnel at GALCIT, 603–610. In: Takayama, K. (Ed.) Shock Waves, Proceedings of the 18th International Symposium on Shock Waves, Sendai, Japan 21-26 July 1992. Springer-Verlag (1992)
28. Hornung, H.G., Pullin, D.I., Ponchaut, N.F.: On the question of universality of imploding shock waves. Acta Mech. **201**, 31–35 (2008)
29. Hosseini, S.H.R., Takayama, K.: Implosion of a spherical shock wave reflected from a spherical wall. J. Fluid Mech. **530**, 223–239 (2005)
30. Jeon, H.: An experimental study of shock wave attenuation. Ph.D. thesis, University of Southern California (2017)
31. Jeon, H., Eliasson, V.: Shock wave interactions with liquid sheets. Exp. Fluids **58**(24), 1–11 (2017)
32. Kandula, M., Freeman, R.: On the interaction and coalescence of spherical blast waves. Shock Waves **18**, 21–33 (2008)
33. Krasik, Y.E., Grinenko, A., Sayapin, A., Efimov, S., Fedotov, A., Gurovich, V.Z., Oreshkin, V.I.: Underwater electrical wire explosion and its applications. IEEE Trans. Plasma Sci. **36**(2), 423–434 (2008)
34. Krasik, Y.E., Fedotov, A., Sheftman, D., Efimov, S., Sayapin, A., Gurovich, V.T., Veksler, D., Bazalitski, G., Gleizer, S., Grinenko, A., Oreshkin, V.I.: Underwater electrical wire explosion. Plasma Sources Sci. Technol. **19**(3), 034020–034029 (2010)
35. Krehl, R., van der Geest, M.: The discovery of the Mach reflection effect and its demonstration in an auditorium. Shock Waves **1**, 3–15 (1991)
36. Lazarus, R.B.: Self-similar solutions for converging shocks and collapsing cavities. SIAM J. Numer. Anal. **18**, 316–371 (1981)
37. Lazarus, R., Richtmyer, R.: Similarity solutions for converging shocks. Technical report, Los Alamos Scientific Laboratory of the University of California, Los Alamos, NM (1977)
38. Lin, S.-C.: Cylindrical shock waves produced by instantaneous energy release. J. Appl. Phys. **25**, 54–57 (1954)
39. Mach, E.: Über den Verlauf der Funkenwellen in der Ebene und im Raum. Sitzungsber Akad Wiss Wien (II. Abth.) **78**, 819–838 (1878)
40. Mach, E., Wosyka, J.: Über einige mechanische Wirkungen des elektrischen Funkens. Sitzungsber Akad Wiss Wien (II Abth) **77**, 44–52 (1875)
41. McGrath, J.R.: Exploding wire research 1774–1963. NRL Memorandum Report 1698, US Naval Research Laboratory (1966)
42. Meier G.: Computerized background-oriented schlieren. Exp. Fluids **33**, 181–187 (2002)
43. Nairne, E.: Electrical experiments by Mr. Edward Nairne, of London, mathematical instrument-maker, made with a machine of his own workmanship, a description of which is prefixed. Philos. Trans. **64**, 79–89 (1774). January 1
44. Oshima, K.: Blast waves produced by exploding wire. Technical report, Aeronautical Research Institute (1960)
45. Ponchaut, N.F., Hornung, H.G., Pullin, D.I., Mouton, C.A.: On imploding cylindrical and spherical shock waves in a perfect gas. J. Fluid Mech. **560**, 103–122 (2006)
46. Qiu, S., Eliasson, V.: Interaction and coalescence of multiple simultaneous and non-simultaneous blast waves. Shock Waves **26**(3), 287–297 (2016)
47. Reichenbach, H.: Contributions of Ernst Mach to fluid mechanics. Ann. Rev. Fluid Mech. **15**, 1–28 (1983)

48. Sakurai, A.: On the propagation and structure of the blast wave, I. J. Phys. Soc. Jpn. **8**(5), 662–669 (1953)
49. Sakurai, A.: On the propagation and structure of the blast wave, II. J. Phys. Soc. Jpn. **9**(2), 256–266 (1954)
50. Sakurai, A.: Chapter: On the propagation of cylindrical shock waves. In: Exploding Wires, vol. 1, pp. 264–270. Plenum, New York (1959)
51. Sedov, L.I.: Propagation of intense (strong) blast waves (in Russian). Prikl. Mat. Mek. **10**, 241 (1946)
52. Sedov, L.I.: Similarity and Dimensional Methods in Mechanics, 10th edn. Academic, New York/CRC Press, Boca Raton (1993)
53. Semenov, A.N., Berezkina, M.K., Krassovskaya, I.V.: Classification of pseudo-steady shock wave reflection types. Shock Waves **22**(4), 307–316 (2012)
54. Settles, G.S.: Schlieren and Shadowgraph Techniques – Visualizing Phenomena in Transparent Media. Springer, New York (2001)
55. Takayama, K., Kleine, H., Grönig, H.: An experimental investigation of the stability of converging cylindrical shock waves in air. Exp. Fluids **5**, 315–322 (1987)
56. Taylor, G.I.: The air wave surrounding an expanding sphere. Proc. R. Soc. Lond. A Math. Phys. Sci. **186**, 273–292 (1946)
57. Taylor, G.I.: The formation of a blast wave by a very intense explosion. I. Theoretical discussion. Proc. R. Soc. Lond. A Math. Phys. Sci. **201**, 159–174 (1950)
58. Taylor, G.I.: The formation of a blast wave by a very intense explosion. II. The atomic explosion of 1945. Proc. R. Soc. Lond. A Math. Phys. Sci. **201**, 159–174 (1950)
59. Toepler, M.: Beobachtung von Metalldampfschichtung bei electrischer Drahtzerstäubung. Annalen der Physik **65**, 873–876 (1898)
60. Veksler, D., Sayapin, A., Efimov, S., Krasik, Y.E.: Characterization of different wire configurations in underwater electrical explosion. IEEE Trans. Plasma Sci. **37**(1), 88–98 (2008)
61. von Neumann, J.: Oblique Reflection of Shocks. It's Explosives Research Report, no. 12. Department of Navy, Washington, DC (1943)
62. von Neumann, J.: The point source solution. Technical report, National Defense Research Committee, Division B Report AM-9 (1947)
63. Wang, C., Qiu, S., Eliasson, V.: Quantitative pressure measurement of shock waves in water using a schlieren-based visualization technique. Exp. Tech. (2013). https://doi.org/10.1111/ext.12068
64. Wang, C., Qiu, S., Eliasson, V.: Investigation of shock wave focusing in water in a logarithmic spiral duct, part 1: Weak coupling. Ocean Eng. **102**, 174–184 (2014)
65. Wang, C., Grunenfelder, L., Patwardhan, R., Qiu, S., Eliasson, V.: Investigation of shock wave focusing in water in a logarithmic spiral duct, part 2: strong coupling. Ocean Eng. **102**, 185–196 (2015)
66. Yadav H.S., Murty D.S., Verma S.N.: Measurement of refractive index of water under high dynamic pressures. J. Appl. Phys. **44**, 2197–2200 (1973)
67. Young, R., Glimm, J., Boston, B.: Proceedings of the Fifth International Workshop on Compressible Turbulent Mixing. World Scientific, Singapore (1996)